Front. Chem. Sci. Eng. 2025, 19(4): 34
https://doi.org/10.1007/s11705-025-2535-4

RESEARCH ARTICLE

Stretchable and conductive lignin hydrogel electrolyte for flexible supercapacitor

He-Fei Wan[1,2,3,4], **Xin Zhao**[1,2,3,4], **Qian Guo**[1,2,3,4], **Ce Gao** (✉)[1,2,3,4], **Run-Cang Sun** (✉)[1,2,3,4]

1 Dalian Jinshiwan Laboratory, Dalian Polytechnic University, Dalian 116034, China
2 The Liaoning Province Key Laboratory of Paper and Pulp Engineering, Dalian Polytechnic University, Dalian 116034, China
3 The Dalian Key Laboratory of High Value Application and Development of Botanical Resources, Dalian Polytechnic University, Dalian 116034, China
4 The Key Laboratory of High Value Utilization of Botanical Resources of China Light Industry, Dalian Polytechnic University, Dalian 116034, China

Abstract Although lignin is the second most abundant forest biomass polymer, it has been largely neglected in hydrogel electrolytes due to its insolubility and inflexibility. In this study, a double-crosslinked hydrogel was prepared using aspartic acid-modified lignin and sodium alginate, significantly improving the mechanical properties. The hydrogel exhibited an exceptional strain of 3008% and a tensile strength of 0.03 MPa, demonstrating its remarkable mechanical properties. In addition, high ionic conductivity (11.7 $mS \cdot cm^{-1}$) was obtained due to the abundant presence of hydrophilic groups in the hydrogel. The hydrogel-assembled supercapacitor manifested an impressive specific capacitance of 39.46 $F \cdot g^{-1}$. Notably, the supercapacitor showed a wide potential window of 0–1.5 V and achieved a maximum energy density of 5.48 $Wh \cdot kg^{-1}$ at the power density of 499.9 $W \cdot kg^{-1}$. The capacitance retention remained at 115% after 10000 charge-discharge cycles. Finally, the coulombic efficiency was almost 100% during the cycles. Upon reaching a bending angle of 90°, the specific capacitance retention remained impressively high at 94%. These results suggest that the supercapacitor cans maintain normal electrochemical performance under extremely harsh conditions.

Keywords aspartic acid modified lignin, double-crosslinked hydrogel electrolytes, high ionic conductivity, supercapacitor

Received November 27, 2024; accepted December 21, 2024;
online March 1, 2025

E-mails: gaoce@dlpu.edu.cn (Gao C.),
rcsun3@dlpu.edu.cn (Sun R.-C.)

1 Introduction

The future trend of organic integration between humans and information lies in the development of flexible electronic technology, enabling the integration of lightweight, ultra-thin, stretchable, wearable electronic equipment with real-time monitoring capabilities [1]. These flexible electronic devices can meet the growing demand for health monitoring, motion tracking, and convenience in life. Supercapacitors are representatives of flexible electronic devices with broad application prospects [2]. Compared with traditional capacitors, they have many advantages, including rapid and reversible charging-discharging, extended cycle life, facile fabrication, and low cost [3]. Nevertheless, the electrodes and electrolytes commonly employed in supercapacitors are non-renewable and non-biodegradable materials, which seriously contradict the principles of green and sustainable development [4]. Furthermore, traditional supercapacitors with liquid electrolytes face inherent challenges, such as poor mechanical properties and grievous device leakage issues, impeding their suitability for wearable and portable electronic devices [5]. Hydrogel electrolytes have attracted enormous interest due to their excellent mechanical properties [6], dimensional stability [7], and cost-effectiveness [8]. By employing water-containing hydrogel as electrolytes, they can also serve as separators simultaneously. Therefore, hydrogel electrolytes effectively integrate the superior ionic conductivity exhibited by liquid electrolytes with the inherent safety and leak-proof characteristics of all-solid electrolytes.

In recent years, hydrogels have emerged as promising electrolytes for supercapacitors. For example, Li et al. [9] employed the dynamic redox reaction between silver ion and lignin to generate numerous free radicals, thereby

facilitating the polymerization of acrylic acid monomers and the subsequent formation of the Ag-LNPs/DES/PAA composite gel. The resulting supercapacitor exhibited a remarkable specific capacitance of 208 $F \cdot g^{-1}$ at 0.5 $A \cdot g^{-1}$. Moreover, the incorporation of lignin conferred exceptional mechanical properties upon the Ag-LNPs/DES/PAA composite, including over 300% tensile strain and compression performance exceeding 350 kPa. Yang et al. [10] developed a modified supramolecular carboxylated chitosan hydrogel electrolyte through free radical graft copolymerization of acrylamide monomers. The supercapacitor constructed with this hydrogel electrolyte exhibited a broad voltage window ranging from 0 to 1.4 V and achieved an energy density of 8.7 $Wh \cdot kg^{-1}$. However, these methods have long reaction steps and low polymerization efficiency, thereby diminishing operational ease.

Lignin, the second most prevalent forest biomass polymer, has attracted considerable attention due to its environmentally friendly nature as an energy source and its potential for efficient conversion into high-value chemicals. Additionally, the distinctive features of lignin, including its highly cross-linking structure and the abundance of carbonyl and phenolic components, make it a promising candidate for electrodes and electrolytes in high-performance supercapacitors [11]. Lignin is the by-product of the pulp industry, and its global annual output is about 70 million tons. However, the utilization rate is less than 10%, with the majority being incinerated for heat energy and some being discarded as waste, leading to environmental pollution [12]. Therefore, the comprehensive utilization of lignin has a high value and significance in turning waste into treasure. For instance, Mondal et al. developed a straightforward and scalable approach to fabricate lignin-incorporated SL-g-PAA-Ni hydrogel electrolytes, which are suitable for anti-freezing applications. The supercapacitor assembled from SL-g-PAA-Ni hydrogel at –20 °C manifested a high specific capacitance of 252 $F \cdot g^{-1}$. It demonstrated an excellent energy density of 26.97 $Wh \cdot kg^{-1}$ at the power density of 2667 $W \cdot kg^{-1}$ and capacitance retention of 96.7% after 3000 consecutive charge-discharge cycles [13]. However, the solubility of lignin in acidic and neutral media poses a challenge to its high-value utilization [14]. Consequently, the problem in preparing lignin hydrogel electrolytes lies in the low reactivity of lignin's functional groups in such conditions [15]. Therefore, it is necessary to chemically modify lignin by introducing hydrophilic groups to enhance its hydrophilicity and reactivity [16].

A novel method was proposed for the hydrophilic modification of lignin through the Mannich reaction, with aspartic acid playing a crucial role in enhancing the hydrophilicity of the modified lignin. Then, the hydrogel was synthesized by free radical polymerization of acrylamide monomers and acrylic acid monomers in the presence of sodium alginate, modified lignin, and ammonium persulphate. The cross-linking between modified lignin and sodium alginate effectively enhanced both the conductivity and ductility properties of the resulting hydrogel. Finally, a symmetric supercapacitor was fabricated by sandwiching activated carbon cloth electrodes with the hydrogel as the electrolyte and carbon cloth as the current collectors. The supercapacitors were subjected to a series of electrochemical characterizations, revealing their excellent electrochemical performance. This study presents a facile and promising research direction for flexible, bendable, and renewable energy-storage devices in the future.

2 Experimental

2.1 Materials

The alkali lignin (AL, M_w = 3139.0 $g \cdot mol^{-1}$) was purchased from Shandong Longlive Bio-technology Co., Ltd., China. Formaldehyde solution (CH_2O, AR, 37%), acrylic acid (AA, AR, ⩾ 99%), ammonium persulphate (APS, AR, ⩾ 99.5%) and acrylamide (AM, AR, ⩾ 99%) were purchased from Shanghai Macklin Biochemical Co., Ltd., China. Ethanol (AR, ⩾ 99.7%), hydrochloric acid (AR, 36 wt %), NaOH (AR, ⩾ 96%), sodium alginate (SA, AR, 90%) and acetylene black (AR, 99%) were bought from Sinopharm Chemical Reagent Co., Ltd., China. Aspartic acid (AR, 98%), KOH (AR, 85%), poly(tetrafluoroethylene) (AR, 25 μm) were purchased from Shanghai Aladdin Reagent Co., Ltd., China. Deionized water came from equipment in the laboratory. All reagents utilized in this study were of analytical grade and were employed without any further purification.

2.2 Preparation of aspartic acid modified lignin (ASPL)

First, 5 g of aspartic acid was dissolved in NaOH aqueous solution with magnetic stirring. Then, 10 g of CH_2O was added and the mixture was named as solution A. Similarly, 5 g AL was dissolved in NaOH aqueous solution and the mixture was named as solution B. Solution A was dropped into solution B slowly at 90 °C for 3 h to promote the Mannich reaction process. Upon successful modification, ASPL was isolated through filtration and subsequently adjusted to neutrality using HCl solution. For further purification, dialysis bags with a molecular weight cut-off of 1000 $g \cdot mol^{-1}$ were utilized to eliminate residual reagents. The dialyzed filtrate was then collected and lyophilized.

2.3 Preparation of aspartic acid modified lignin/sodium alginate double crosslinked hydrogel electrolyte (ASH)

First, 1 g sodium alginate was dissolved in KOH solution

(3 mol·L^{-1}, 100 mL) under vigorously stirring for 12 h to prepare homogeneous solution. ASPL was added to the above solution. Then, 1 g of acrylic acid and 1 g of acrylamide were sequentially added to above mixture and stirred at room temperature for a while. Next, proper amount of APS was added into the mixture. The homogeneous solution was transferred to an oven and kept at 60 °C for 1 h. Following these steps, the lignin-based composite hydrogel electrolyte was synthesized. For comparison, other operations were same as above and the hydrogel prepared with AL was named ALH. Similarly, the hydrogel prepared without lignin was named AH. In addition, the preparing of electrodes and assembling of supercapacitors are listed in the Electronic Supplementary Material (ESM).

3 Results and discussion

3.1 Structural analysis of ASPL and ASH

The comprehensive synthesis pathway for ASH was illustrated in Scheme 1. AL was modified by the Mannich reaction to produce ASPL, which has significant hydrophilicity [17,18]. Additionally, Fig. 1(a) provides a comprehensive visualization of the Mannich reaction mechanism [19]. Figure 1(b) depicts the ^{1}H nuclear magnetic resonance (NMR) spectrum of AL and ASPL. The proton signals corresponding to the aromatic and aliphatic regions of lignin were observed at δ 6.0–8.0 ppm and δ 2.0–4.0 ppm, respectively, indicating that the primary structure of lignin maintained stability throughout the Mannich reaction process [20]. Moreover, the proton signals in the aliphatic regions of ASPL were much stronger than AL, providing compelling evidence for the successful grafting of amino acid groups onto ASPL and the successful preparation of ASPL [21].

The Fourier transform infrared spectroscopy (FTIR) results are presented in Fig. 2. The signals observed at 3408 and 2940 cm^{-1} in spectra of AL and ASPL corresponded to the stretching vibrations of O–H and C–H bonds, respectively [22]. The findings demonstrated a significant preservation of the primary structures of lignin throughout the Mannich reaction, which was consistent with the results obtained from the ^{1}H NMR spectrum. Notably, a novel peak at 1384 cm^{-1} emerged in both the ASPL and ASH spectra compared to the AL spectrum. This peak was attributed to the stretching vibration of the C–N bond, indicating the successful introduction of nitrogen-containing functionalities through the Mannich reaction [23]. Furthermore, the ASH spectrum presented a distinctive signal peak at 1674 cm^{-1}, which was absent in other spectra. This signal could be attributed to the C=O stretching vibration of –COOR, indicating the presence of AA in ASH [24].

Figure 3 depicts the XPS spectroscopy of ASPL and

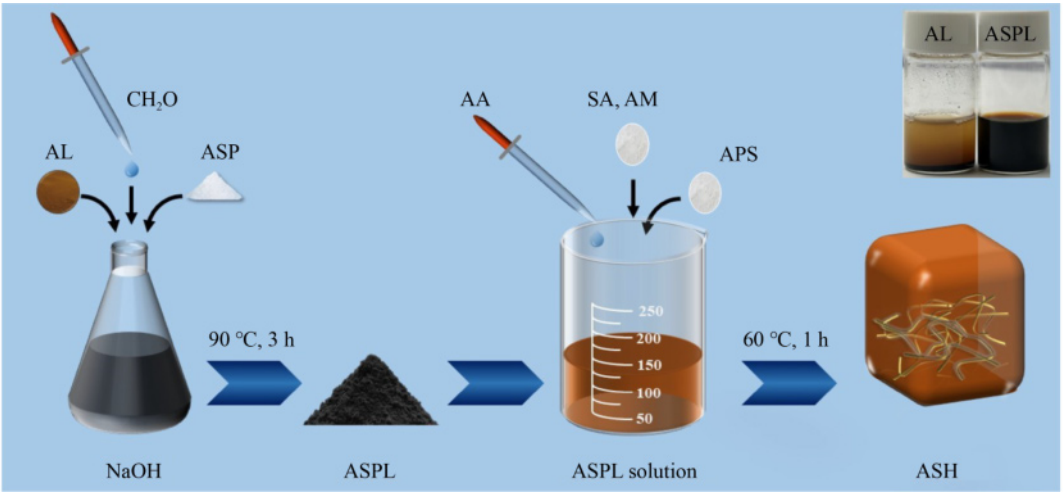

Scheme 1 The comprehensive synthesis pathway for ASH.

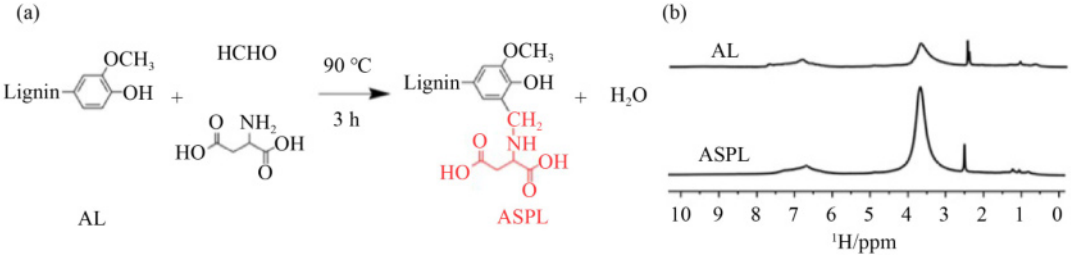

Fig. 1 (a) Mannich reaction mechanism of amino acid-modified lignin; (b) ^{1}H NMR spectrum of AL and ASPL.

ASH. The characteristic peaks at 533.7, 400.8, and 285.9 eV were assigned to the O 1s, N 1s, and C 1s diffraction signals, respectively. These results indicate the presence of abundant functional groups containing oxygen, nitrogen, and carbon in both ASPL and ASH. The detection of nitrogen elements in both ASPL and ASH confirms the successful occurrence of the Mannich reaction. Furthermore, peak fitting was conducted on the C 1s and N 1s diffraction peaks, resulting in three distinct peaks observed in high-resolution C 1s XPS spectra of ASPL and ASH: specifically at energies of 288.1 eV (C=O), 286.3 eV (C–N), and 284.8 eV (C–C/C–H) (Fig. 3(b) and Fig. 3(e)) [25,26]. Compared to ASPL, the diffraction peak area of C=O in ASH was significantly enlarged due to the carboxyl groups introduced from AA. As shown in Figs. 3(c, f), the high-resolution N 1s spectra exhibited two distinct peaks at 401.5 and 399.5 eV, corresponding to the N–H groups and C–N groups, respectively [27,28]. The presence of the N–H group was derived from the amino group of aspartic acid, and C–N represented a novel bond in the Mannich reaction. Additionally, K 2p and S 2p were also detected in the XPS survey spectra of ASH, which were residues of KOH and APS reagents.

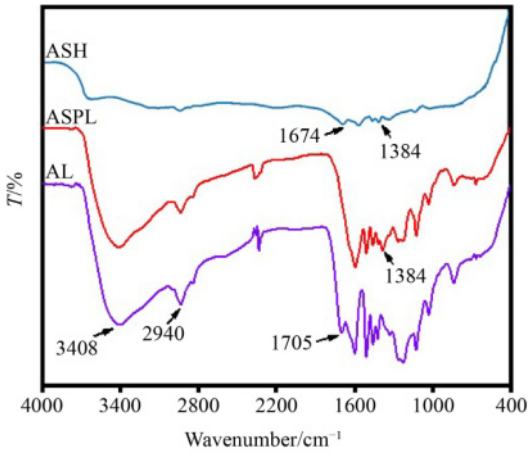

Fig. 2 FTIR spectra of AL, ASPL, and ASH.

3.2 Characterization of hydrogel electrolytes

As illustrated in Fig. 4(a), the ASH hydrogel exhibited a well-developed network structure, with abundant pores indicating its porous nature. Figure 4(b) shows the corresponding enlarged image, demonstrating that the network structure was full of white crystals. The statistical results after energy dispersive X-ray spectral analysis (EDS) are shown in Figs. 4(c–f). The appearance of the K element indicated that the white crystals in the developed network structure were KOH. Subsequent freeze-drying resulted in the formation of these white crystals due to water loss from KOH. As the liquid component of ASH, KOH provided a suitable solution system for lignin and improved the electrochemical performance [29]. The results revealed the uniform distribution of the electrolyte solution within the developed pore structure, with the K element appearing on the surface and inside of the pore structure [30]. The presence of the N element indicated the successful cross-linking of ASPL with sodium alginate, acrylamide, and acrylic acid to form a double cross-linked network structure. The introduction of ASPL endowed ASH with good hydrophilic and electrochemical properties.

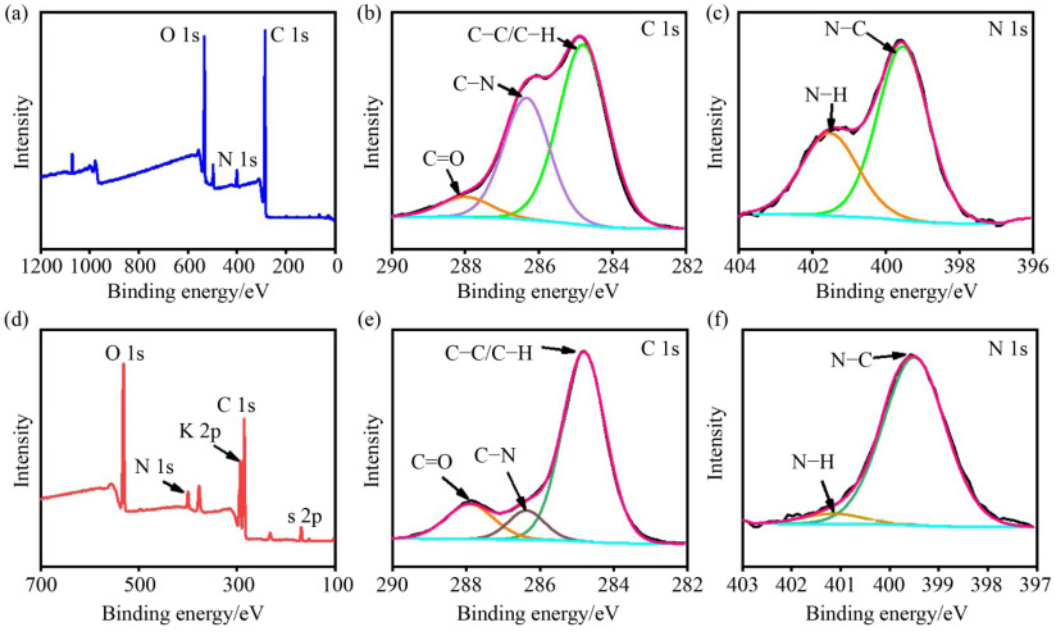

Fig. 3 (a) XPS survey spectra of ASPL; (b) high-resolution C 1s and (c) N 1s XPS spectra of ASPL; (d) XPS survey spectra of ASH; (e) high-resolution C 1s and (f) N 1s XPS spectra of ASH.

Additionally, the uniform distribution of the N element illustrated even grafting of reactants and a uniform during the Mannich reaction [31]. The S element was the residue of APS reagents. The corresponding element contents of ASH hydrogel electrolyte are shown in Fig. S2 (cf. ESM). The elemental analysis of ASH indicated that it primarily consisted of C at 45.19%, O at 28.5%, K at 19.72%, N at 4.78%, and S at 1.82%. Furthermore, the FE-SEM and SEM-EDS elemental mapping techniques provided conclusive evidence for the successful synthesis of ASPL and the creation of a lignin-based network composite hydrogel electrolyte.

The comparison of mechanical properties of hydrogel electrolytes is illustrated in Fig. 5(a). At an initial length of the hydrogel of 10 mm and an elongation rate of 10 mm·min^{-1}, the maximum tensile length of ASH reached 300.8 mm and a corresponding strain of 3008% after three tests. Under the same conditions, the ALH exhibited a maximum tensile length of 260.1 mm with a corresponding strain of 2601%. Similarly, the maximum tensile length of AH was 274.8 mm, and the strain reached 2748%. In addition, the tensile strength of ASH and ALH were 0.03 MPa and 0.024 MPa, respectively, which were higher than that of AH (0.013 MPa). The results demonstrated that the incorporation of lignin led to the formation of a cross-linked network structure, which exhibited enhanced tensile strength. However, the bonding of AL with acrylamide and acrylic acid decreased the ductility of the hydrogel network, resulting in a decrease in fracture strain compared with AH [32]. Remarkably, ASH exhibited the highest fracture strain, indicating that aspartic acid occupied part of the active sites and reduced the connection with acrylamide and acrylic acid [33]. Moreover, the increase of –NH– and –COOH functional groups augmented the number of hydrogen bonds within ASH, thereby enhancing its ductility [34,35]. As shown in Fig. S3 (cf. ESM), ASH had the highest toughness (0.54 MJ·m^{-3}), which was consistent with the conclusions of the tensile stress-strain curves. ASH exhibited remarkable tensile strength and strain resistance, thereby demonstrating its exceptional mechanical properties. This result suggests that introducing a large number of hydrophilic functional groups can effectively enhance the toughness of ASH. Simultaneously, Fig. S4 (cf. ESM) illustrates the elastic modulus of the ASH, ALH, and AH. The minimum elastic modulus (0.66 kPa) of ASH indicated excellent flexibility compared with ALH (1.26 kPa) and AH (0.95 kPa), satisfying the current requirements for flexible electrolytes. Thermal stability experiments were performed using thermogravimetric analysis (TGA-DTG, Fig. 5(b)). The three curves had different weight loss rates after 100 °C, and the weight loss was ascribed to the evaporation of free water inside the hydrogel. The introduction of –NH– and –COOH hydrophilic functional groups resulted in different weight loss rates, indicating an increased number of hydrogen bonds within ASH. Therefore, the water binding ability of ASH was stronger than ALH. At 300 °C, the weight retention of ASH was 80%, significantly higher than that of ALH (67%). The comparison of TGA-DTG curves highlighted the exceptional thermal stability of ASH, which was crucial for enhancing the electrochemical stability of supercapacitors.

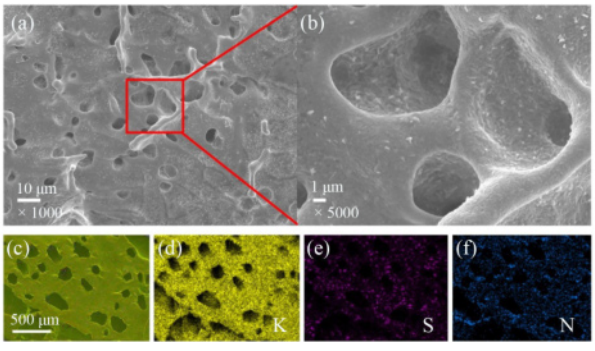

Fig. 4 (a, b) FE-SEM images of ASH; (c–f) SEM-EDS elemental mappings.

3.3 Electrochemical performance

The Nyquist plots (Fig. 6(a)) illustrate the values of equivalent series resistance (ESR), which were determined by intersecting the EIS curve with the real

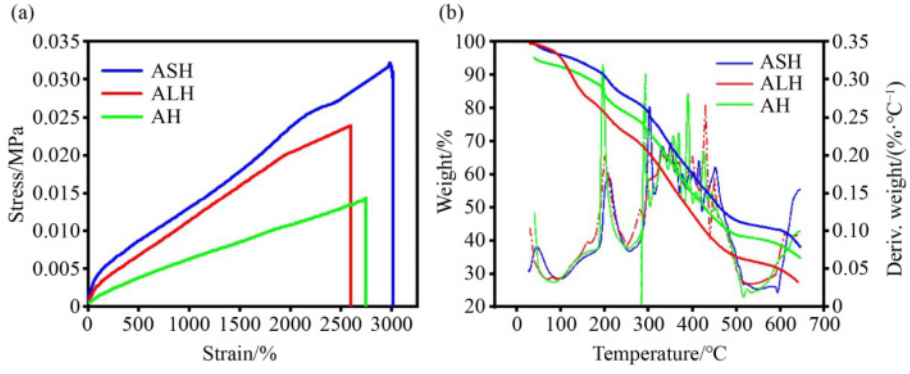

Fig. 5 (a) Tensile stress-strain curves of the ASH, ALH and AH; (b) TGA-DTG curves of hydrogel electrolytes.

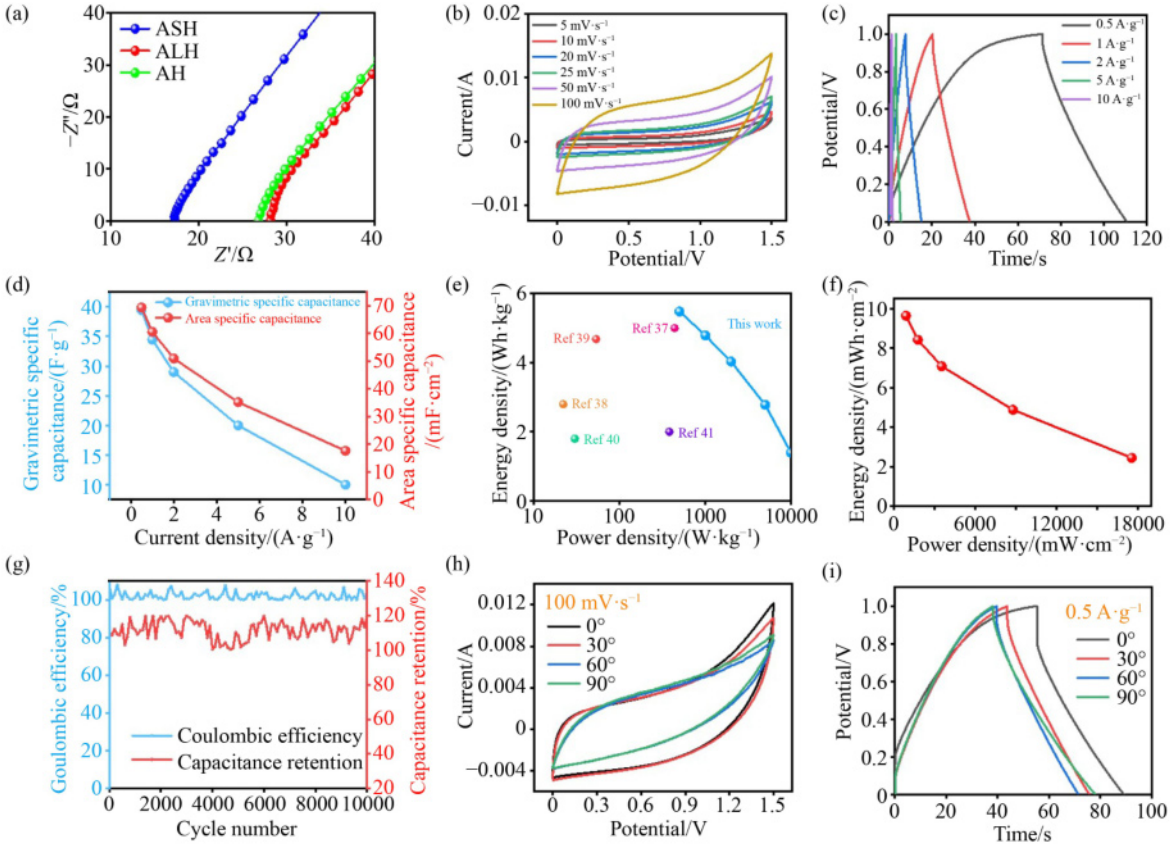

Fig. 6 (a) EIS curves of ASH, ALH and AH; (b) CV curves at 5 mV·s^{-1} to 100 mV·s^{-1} scan rates; (c) GCD curve measured at each current density; (d) relation between specific capacitance and current density; (e, f) the Reagon plots; (g) cycling stability; (h) CV curves in different bending angles at scan rate of 100 mV·s^{-1}; (i) GCD curves in different bending angles at current density of 0.5 A·g^{-1}.

axis in the high-frequency region, were 17.1, 26.3 and 28.4 Ω for ASH, AH, and ALH, respectively. A lower ESR suggested a closer approximation of the device to an ideal capacitor behavior [36]. Consequently, ASH electrolytes possessed rapid ion transport channels. The ionic conductivity of hydrogel electrolytes is shown in Fig. S5 (cf. ESM). Specifically, the ionic conductivity of ASH was 11.7 mS·cm^{-1}, higher than that of AH (7.6 mS·cm^{-1}) and ALH (7.1 mS·cm^{-1}). High ionic conductivity could be attributed to the abundant hydrophilic groups in ASH. Moreover, the Nyquist plot revealed an arcuate profile in the high-frequency domain and a linear trend in the low-frequency domain, demonstrating the characteristic capacitive nature of hydrogel [37]. Figure S6 (cf. ESM) was obtained through simulation using ZSimDemo software. It can be seen that the actual data of the hydrogel electrolytes were highly consistent with the simulation data, suggesting the excellent electrochemical performance of hydrogel electrolytes. The simulated circuit of ASH is presented at the bottom right of the diagram. The charge transfer resistance (R_{ct}) was determined by extrapolating the diameter of the semicircle observed in the high-frequency region. Notably, the R_{ct} value for ASH was 22.02 Ω, substantially lower than those of ALH (45.72 Ω) and AH (61.04 Ω). The R_{ct} was primarily influenced by the inherent properties of the electrode material and the conductivity of the electrolyte. Consequently, a reduced R_{ct} value indicated a beneficial interfacial effect. ESR and R_{ct} values suggested that ASH facilitated more efficient charge transfer and ion diffusion at the electrolyte-electrode interface, thereby exhibiting excellent conductivity properties.

The effect of varying KOH concentrations on the equivalent series resistances of the electrolyte is shown in Fig. S7 (cf. ESM). The equivalent series resistances increased with increasing KOH concentration. Therefore, 3 mol·L^{-1} KOH was selected as the solvent for the following characterizations. The electrochemical properties of the supercapacitor were subsequently evaluated. Figure 6(b) shows the CV curves using the potential window of 0 to 1.5 V and scan rates of 5 to 100 mV·s^{-1}. The CV curves remained a quasi-parallelogram shape without significant distortion even at a high scan rate of 100 mV·s^{-1}, suggesting the rapid ion transport rate and low charge transfer resistance of the supercapacitor. In addition, the areas of CV curves increased with increasing scan rates, demonstrating the excellent rate capability of the supercapacitor. The GCD measurement was conducted at various current densities, as depicted in

Fig. 6(c). The symmetric triangular shape observed in the GCD curves within the range of 0.5 to 10 $A \cdot g^{-1}$ further verified the exceptional charge-discharge reversibility of the supercapacitor. Figure 6(d) exhibited the specific capacitance plots with increasing current density. According to the GCD curves, a maximum gravimetric specific capacitance of 39.46 $F \cdot g^{-1}$ at the current density of 0.5 $A \cdot g^{-1}$ was obtained using Eq. (2). Similarly, the maximum area specific capacitance was 69.4 $mF \cdot cm^{-2}$. The Ragone plots in Figs. 6(e, f) depict the relationship between energy density and power density. The supercapacitor demonstrated a maximum energy density of 5.48 $Wh \cdot kg^{-1}$ at a power density of 499.9 $W \cdot kg^{-1}$. Notably, it maintained an energy density of 1.39 $Wh \cdot kg^{-1}$ even at an ultrahigh power density of 10.1 $kW \cdot kg^{-1}$. The supercapacitor delivered a high areal energy density of 9.64 $mWh \cdot cm^{-2}$ at the power density of 879 $mW \cdot cm^{-2}$. Compared to previous studies, the supercapacitor in this work exhibited superior electrochemical performance [37−41]. It showed excellent capacitance retention of 115% after 10000 charging and discharging cycles (Fig. 6(g)), and its coulombic efficiency was very close to 100%. These results underscored the excellent recycling capability of the supercapacitor. Figures 6(h, i) showed the CV and GCD plots at different bending angles at the scan rate of 100 $mV \cdot s^{-1}$ and the current density of 0.5 $A \cdot g^{-1}$, respectively. At varying bending angles, the CV curves remained largely coincident, while the GCD curves indicated comparable charge and discharge times. In addition, at the bending angle of 90°, the specific capacitance retention remained impressively high at 94%, proving the excellent adaptability and resilience of the supercapacitor under extreme conditions. Figure 7(a) shows a timer powered by one supercapacitor for three minutes. Three supercapacitors connected in series could continuously light an LED bulb for 70 s (Fig. 7(b)). Therefore, the supercapacitor can satisfy the actual power demand and has great potential in practical applications.

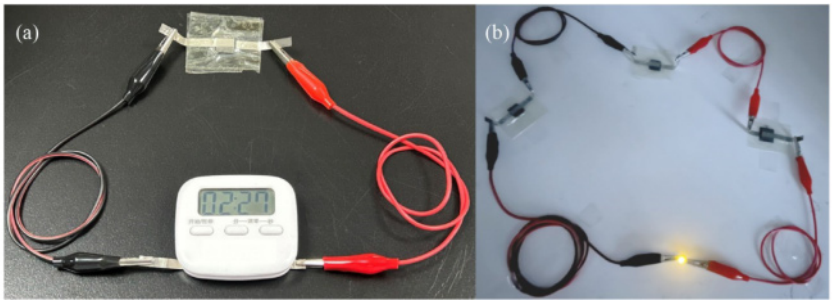

Fig. 7 (a) Picture of timer powered by one supercapacitor for a few minutes; (b) picture of LED lamp powered by three supercapacitors.

4 Conclusions

This study proposes a new method for the hydrophilic modification of lignin. The lignin-based network composite hydrogel is prepared through free radical polymerization. After adding ASPL, the conductive and mechanical properties of ASH are significantly enhanced. The ASH exhibits an exceptional strain of 3008%, along with a tensile strength of 0.03 MPa. Moreover, the high ionic conductivity of ASH leads to excellent electrochemical properties. The supercapacitor has a specific capacitance of 39.46 $F \cdot g^{-1}$ with a maximum energy density of 5.48 $Wh \cdot kg^{-1}$. More importantly, the supercapacitor exhibits a stable rate and recycling performance, which is conducive to the fabrication of next-generation renewable energy equipment.

Acknowledgements The authors acknowledge the financial support from the National Natural Science Foundation of China (Grant No. 51961125207), and the Foundation (Grant No. KF202114) of Key Laboratory of Pulp and Paper Science & Technology of Ministry of Education, Qilu University of Technology (Shandong Academy of Sciences), and Dalian High Level Talent Innovation Support Program (Dalian Youth Science and Technology Star Project Support Program) (Grant No. 2023RQ043), and Open Foundation of Dalian Jinshiwan Laboratory (Grant No. Dljswkf202412), and Basic Scientific Research Project of Liaoning Provincial Department of Education (Grant No. LJ212410152015), and Introduction of Talent Research Start-up Funding Projects (Dalian Polytechnic University, Grant No. LJBKY2024013).

Electronic Supplementary Material Supplementary material is available in the online version of this article at https://doi.org/10.1007/s11705-025-2535-4 and is accessible for authorized users.

Competing interests The authors declare that they have no competing interests.

References

1. Dong X, Chen W, Ge X, Li S, Xing Z, Zhang Q, Wang Z. Stretchable, self-adhesion and durable polyacrylamide/polyvinylalcohol dual-network hydrogel for flexible supercapacitor and wearable sensor. Journal of Energy Storage, 2024, 89: 111793
2. Liu Y, Wang X, Abdiryim T, Jamal R, Liu X, Xu F, Liu F, Fan N, Song K, Yang H. Polythiophene Coating-encapsulated $CoNi_2S_4$@HCS for quasi-solid-state hybrid supercapacitors with gel electrolyte containing gelatin. Carbon, 2024, 218: 118736

3. Chen C, Li Y, Qian C, Liu X, Yang Y, Han L, Han Q. Carboxymethyl cellulose assisted PEDOT in polyacrylamide hydrogel for high performance supercapacitors and self-powered sensing system. European Polymer Journal, 2022, 179: 111563
4. Li Y, Zhou X, Sarkar B, Gagnon-Lafrenais N, Cicoira F. Recent progress on self-healable conducting polymers. Advanced Materials, 2022, 34(24): 2108932
5. Wu X, Zeng F, Song X, Sha X, Zhou H, Zhang X, Liu Z, Yu M, Jiang C. *In-situ* growth of $Ni(OH)_2$ nanoplates on highly oxidized graphene for all-solid-state flexible supercapacitors. Chemical Engineering Journal, 2023, 456: 140947
6. Ghosh S, Majhi J, Sharma S, Priya K, Bandyopadhyay A. A review on the development of electron and ion conductive polymer hydrogels and their composites for flexible and smart supercapacitors. Journal of Energy Storage, 2023, 74: 109423
7. Fei Y, Jiang Z, Zhou D, Meng F, Wu Y, Xiong Y, Ye Y, Liu T, Fei Z, Kuang T, et al. Preparation a highly sensitive and flexible textile supercapacitor based on lignin hydrogel and polyaniline@carbon cloth composites. Journal of Energy Storage, 2023, 73: 108978
8. Moyer-Vanderburgh K, Park S J, Fornasiero F. Growth of carbon nanotube forests on flexible metal substrates: advances, challenges, and applications. Carbon, 2023, 206: 402–421
9. Li T, Wang S, Huang Y, Zhou H, Zhang L, Wang Z. Lignin-induced rapid-synthesis of deep eutectic solvent-based gel with high robustness and conductivity applied for flexible quasi-solid-state supercapacitors. Chemical Engineering Journal, 2023, 472: 144864
10. Yang H, Ji X, Tan Y, Liu Y, Ran F. Modified supramolecular carboxylated chitosan as hydrogel electrolyte for quasi-solid-state supercapacitors. Journal of Power Sources, 2019, 441: 227174
11. Wang S, Shi Y, Chen S, Zhu C, Wang X, Zhou T, Su L, Tan C, Zhang L, Xiang H. Porous biochars with nitrogen defects prepared from hydrogel template-modified food waste for high-performance supercapacitors. Journal of Energy Storage, 2023, 72: 108720
12. Lian Y, Yu G, Lu L, Guo H, Wang J, Dai Y, Tang X, Zhang H. Controllable thickness carbon sheet under anion and cation co-doping for supercapacitors and capacitive deionization. Carbon, 2024, 225: 119097
13. Mondal A K, Xu D, Wu S, Zou Q, Lin W, Huang F, Ni Y. Lignin-containing hydrogels with anti-freezing, excellent water retention and super-flexibility for sensor and supercapacitor applications. International Journal of Biological Macromolecules, 2022, 214: 77–90
14. Salinas-Torres D, Ruiz-Rosas R, Morallón E, Cazorla-Amorós D. Strategies to enhance the performance of electrochemical capacitors based on carbon materials. Frontiers in Materials, 2019, 6: 115
15. Deghiedy N M, Yousif N M, Hosni H M, Balboul M R. Silver-modified electrodes based on amorphous MnO_2/carbon nanotube: multicomponent approach to enhance the performance of supercapacitors. Journal of Physics and Chemistry of Solids, 2022, 161: 110445
16. Khan M S, Jhankal D, Shakya P, Sharma A K, Banerjee M K, Sachdev K. Ultraslim and highly flexible supercapacitor based on chemical vapor deposited nitrogen-doped bernal graphene for wearable electronics. Carbon, 2023, 208: 227–237
17. Shang M, Zhang X, Zhang J, Sun J, Zhao X, Yu S, Liu X, Liu B, Yi X. Nitrogen-doped carbon composite derived from ZIF-8/polyaniline@ cellulose-derived carbon aerogel for high-performance symmetric supercapacitors. Carbohydrate Polymers, 2021, 262: 117966
18. Nz M, Rahmanifar M, Noori A. The ordered mesoporous carbon nitride-graphene aerogel nanocomposite for high-performance supercapacitors. Journal of Power Sources, 2021, 494: 229741
19. Du X, Li J, Lindström M E. Modification of industrial softwood kraft lignin using Mannich reaction with and without phenolation pretreatment. Industrial Crops and Products, 2014, 52: 729–735
20. Sardana S, Gupta A, Singh K, Maan A S, Ohlan A. Conducting polymer hydrogel based electrode materials for supercapacitor applications. Journal of Energy Storage, 2022, 45: 103510
21. Tana T, Zhang Z, Moghaddam L, Rackemann D W, Rencoret J, Gutiérrez A, Del Río J C, Doherty W O. Structural changes of sugar cane bagasse lignin during cellulosic ethanol production process. ACS Sustainable Chemistry & Engineering, 2016, 4(10): 5483–5494
22. Huang J, Hu Y, Wang H, Wang T, Wu H, Li J, Li Y, Wang M, Zhang J. Lignin isolated from poplar wood for porous carbons as electrode for high-energy renewable supercapacitor driven by lignin/deep eutectic solvent composite gel polymer electrolyte. ACS Applied Energy Materials, 2022, 5(5): 6393–6400
23. Bélteki R, Kuklis L, Gombár G, Ungor D, Csapó E. The role of the amino acid molecular characteristics on the formation of fluorescent gold- and silver-based nanoclusters. Chemistry, 2023, 29(45): e202300720
24. Fan X, Wang X, Cai Y, Xie H, Han S, Hao C. Functionalized cotton charcoal/chitosan biomass-based hydrogel for capturing Pb^{2+}, Cu^{2+} and MB. Journal of Hazardous Materials, 2022, 423: 127191
25. Tian W, Gao Q, Zhang L, Yang C, Li Z, Tan Y, Qian W, Zhang H. Renewable graphene-like nitrogen-doped carbon nanosheets as supercapacitor electrodes with integrated high energy-power properties. Journal of Materials Chemistry A: Materials for Energy and Sustainability, 2016, 4(22): 8690–8699
26. Tian W, Gao Q, Tan Y, Yang K, Zhu L, Yang C, Zhang H. Bio-inspired beehive-like hierarchical nanoporous carbon derived from bamboo-based industrial by-product as a high performance supercapacitor electrode material. Journal of Materials Chemistry A: Materials for Energy and Sustainability, 2015, 3(10): 5656–5664
27. Pour-Ali S, Tavangar R, Hejazi S. Comprehensive assessment of some L-amino acids as eco-friendly corrosion inhibitors for mild steel in HCl: insights from experimental and theoretical studies. Journal of Physics and Chemistry of Solids, 2023, 181: 111550
28. Zhang W, Li H J, Wang M, Wang L J, Pan Q, Ji X, Qin Y, Wu Y C. Tetrahydroacridines as corrosion inhibitor for X80 steel corrosion in simulated acidic oilfield water. Journal of Molecular Liquids, 2019, 293: 111478
29. Gao M, Wang L, Zhao B, Gu X, Li T, Huang L, Wu Q, Yu S, Liu S. Sandwich construction of chitosan/reduced graphene oxide composite as additive-free electrode material for high-

performance supercapacitors. Carbohydrate Polymers, 2021, 255: 117397

30. Fang H, Xie X, Chu Q, Tong W, Song K. Modified 1,4-butanediol organosolv pretreatment on hardwood and softwood for efficient coproduction of fermentable sugars and lignin antioxidants. Bioresource Technology, 2023, 376: 128854
31. Zhang J, Zhuang J, Lei L, Hou Y. Rapid preparation of a self-adhesive PAA ionic hydrogel using lignin sulfonate-Al^{3+} composite systems for flexible moisture-electric generators. Journal of Materials Chemistry A: Materials for Energy and Sustainability, 2023, 11(7): 3546–3555
32. Zhang K, Pang Y, Chen C, Wu M, Liu Y, Yu S, Li L, Ji Z, Pang J. Stretchable and conductive cellulose hydrogel electrolytes for flexible and foldable solid-state supercapacitors. Carbohydrate Polymers, 2022, 293: 119673
33. Omar K A, Sadeghi R. Physicochemical properties of deep eutectic solvents: a review. Journal of Molecular Liquids, 2022, 360: 119524
34. Wang Z, Pan Q. An omni-healable supercapacitor integrated in dynamically cross-linked polymer networks. Advanced Functional Materials, 2017, 27(24): 1700690
35. Guo Y, Zheng K, Wan P. A flexible stretchable hydrogel electrolyte for healable all-in-one configured supercapacitors. Small, 2018, 14(14): 1704497
36. Zeng J, Dong L, Sha W, Wei L, Guo X. Highly stretchable, compressible and arbitrarily deformable all-hydrogel soft supercapacitors. Chemical Engineering Journal, 2020, 383: 123098
37. Attias R, Sharon D, Borenstein A, Malka D, Hana O, Luski S, Aurbach D. Asymmetric supercapacitors using chemically prepared MnO_2 as positive electrode materials. Journal of the Electrochemical Society, 2017, 164(9): A2231–A2237
38. Bashir S, Omar F S, Hina M, Numan A, Iqbal J, Ramesh S, Ramesh K. Synthesis and characterization of hybrid poly (*N*,*N*-dimethylacrylamide) composite hydrogel electrolytes and their performance in supercapacitor. Electrochimica Acta, 2020, 332: 135438
39. Liu Y, Zhou H, Zhou W, Meng S, Qi C, Liu Z, Kong T. Biocompatible, high-performance, wet-adhesive, stretchable all-hydrogel supercapacitor implant based on PANI@ rGO/Mxenes electrode and hydrogel electrolyte. Advanced Energy Materials, 2021, 11(30): 2101329
40. Lin T, Shi M, Huang F, Peng J, Bai Q, Li J, Zhai M. One-pot synthesis of a double-network hydrogel electrolyte with extraordinarily excellent mechanical properties for a highly compressible and bendable flexible supercapacitor. ACS Applied Materials & Interfaces, 2018, 10(35): 29684–29693
41. Tao F, Qin L, Wang Z, Pan Q. Self-healable and cold-resistant supercapacitor based on a multifunctional hydrogel electrolyte. ACS Applied Materials & Interfaces, 2017, 9(18): 15541–15548